

Learning Policies for Dynamic Coalition Formation in Multi-Robot Task Allocation

Lucas C. D. Bezerra , Ataíde M. G. dos Santos , and Shinkyu Park 

Abstract—We propose a decentralized, learning-based framework for dynamic coalition formation in Multi-Robot Task Allocation (MRTA). Our approach extends Multi-Agent Proximal Policy Optimization (MAPPO) by incorporating spatial action maps, robot motion control, task allocation revision, and intention sharing to enable effective coalition formation. Extensive simulations demonstrate that our model significantly outperforms existing methods, including a market-based baseline. Furthermore, we assess the scalability and generalizability of the proposed framework, highlighting its ability to handle large robot populations and adapt to diverse task allocation environments.

I. INTRODUCTION

Coalition formation, widely observed in nature, such as in ant colonies and bee hives, inspires researchers and engineers to design simple robots capable of strategic cooperation. In multi-robot systems, coalitions emerge when the collective actions of robots exceed what they could accomplish individually, as illustrated in Fig. 1. In this work, we focus on developing a team of robots capable of performing tasks that require coalition in dynamic environments. In such scenarios, robots must learn to coordinate by leveraging both local information gathered from their own sensors and shared data from neighboring robots to effectively execute complex multi-robot tasks.

Multi-Robot Task Allocation (MRTA) is a research theme directly relevant to our work, which seeks to address the challenge of assigning and executing multiple tasks across a team of robots to optimize a collective objective. We focus on MRTA problems characterized by: (i) each robot being capable of executing one task at a time, (ii) tasks requiring multiple robots simultaneously to be completed, and (iii) robots needing to be adjacent to a task to execute it, requiring movement to the task location beforehand. This problem formulation falls under the Single-Task robots, Multi-Robot tasks, Time-extended Assignment (ST-MR-TA) category of MRTA, as defined by the taxonomy in [1]. Relevant applications include transportation [2] and service dispatch scenarios [3], [4] such as firefighting and large-scale disaster response.

The work was supported by funding from King Abdullah University of Science and Technology (KAUST).

Bezerra and Park are with Electrical and Computer Engineering, King Abdullah University of Science and Technology (KAUST), Thuwal, 23955-6900, Kingdom of Saudi Arabia. {lucas.camaradantasbezerra, shinkyu.park}@kaust.edu.sa

Santos is with the Postgraduate Program in Electrical Engineering, PROEE, Federal University of Sergipe (UFS), São Cristóvão, Sergipe, 49107-230, Brazil. ataidegualberto.eng@gmail.com



Fig. 1: The firetruck dispatch is an illustrative example of a dynamic coalition formation problem: without a centralized coordinator, a team of firetrucks must form coalitions in a decentralized fashion to tackle tasks, such as extinguishing fires, that cannot be accomplished individually.

We focus on developing a decentralized solution where each robot observes only its immediate surroundings. With such partial observability in MRTA, robots only identify tasks within their sensor range, causing the set of perceived tasks to change as they move. Additionally, we consider dynamic environments where new tasks continuously emerge over time. Well-established approaches to partially observable task allocation problems rely on inter-robot communication, where robots share their observations, internal state, and decision with their neighbors. Market-based approaches [5], [6] are among the most popular frameworks due to their robustness and scalability. However, these methods often rely on high-frequency communication for information exchange between robots to reach agreement before task assignments are made [6]–[8]. Although this strategy is efficient in some restricted cases, it becomes impractical in dynamic environments.

We propose a learning-based framework for multi-robot dynamic coalition formation to address problems within the ST-MR-TA MRTA category. In this framework, each robot utilizes a receding horizon-type planning strategy to generate a long-term plan for task execution, which is repeatedly revised as necessary in subsequent time steps. The robot shares the plan with other robots that are within its communication range. This combination of task reassessment and sharing of the task execution plan enables dynamic coalition formation. Our contributions are summarized as follows:

- (i) To the best of our knowledge, this is the first work to tackle the problem of decentralized dynamic coalition formation under partial observability. To facilitate coalition, we extend a Multi-Agent Reinforcement Learning (MARL) algorithm by integrating receding horizon task planning and communication of an intention map, which captures the information on the task execution plan.

- (ii) Each robot’s policy is modeled as an end-to-end convolutional neural network based on the U-Net architecture [9]. The network processes task information within the robot’s sensing range and incorporates the intentions of neighboring robots. This shared network is trained using the MAPPO algorithm and then distributed across all robots.
- (iii) Through extensive simulations, we demonstrate that our approach outperforms existing methods including the market-based approach, PCFA. Additionally, we demonstrate the scalability of models up to 1000 robots and their generalizability across a wide range of task settings.

This paper is organized as follows: §II reviews related work in MRTA and MARL. In §III, we formally define the problem of dynamic coalition formation as a Dec-POMDP. §IV outlines our proposed method as a solution to the problem. In §V, we evaluate the effectiveness, scalability, and generalizability of the proposed method through extensive simulations, comparing it to the baseline. §VI summarizes the paper and outlines future research directions.

II. RELATED WORK

Solutions to ST-MR-TA MRTA include optimization-based [10]–[13], trait-based [14], [15], and market-based [6]–[8], [16] methods. Among decentralized solutions for MRTA, market-based approaches are particularly popular. Specifically, the PCFA [8] is a market-based solution designed for coalition formation in homogeneous teams with dynamic tasks. Due to the similarity in problem formulation, we selected PCFA as the baseline for our simulations reported in §V.

Reinforcement Learning (RL) focuses on learning a policy (i.e., a mapping from observations to actions) that maximizes a robot’s total reward in a Markov decision process. It has been widely applied to various robotics problems, particularly in object manipulation [17]–[21]. While many approaches aim to directly control robot actuators, studies such as [17], [18], [22] propose the use of an abstract action map. In this framework, the policy selects a task at each step, while a motion planner handles the low-level actuator control to navigate the robot to the task location. This abstraction alleviates the learned policy from handling low-level control, allowing it to concentrate on long-term planning.

This approach is extended to the multi-robot domain in [23], where robots not only select task locations but also communicate their chosen task locations to nearby robots. The authors show that this additional communication improves cooperation and enhances overall performance. However, their method does not address coalition formation. As demonstrated in §V, their approach, with appropriate adaptations, performs suboptimally compared to ours in scenarios that require effective coalition formation. MARL naturally extends the conventional RL framework to cooperative multi-robot scenarios, where instead of learning policies to maximize individual rewards, robots learn to maximize a global reward through coordination [24]. Several studies have

adapted RL algorithms for the multi-robot domain [25]–[33]. A widely adopted approach is the Centralized Training and Decentralized Execution (CTDE) paradigm, where robots are trained using shared information [27]–[33]. CTDE offers faster training and addresses non-stationarity, a significant challenge in MARL.

Several studies have applied MARL to MRTA [23], [29], [34], [35], but only [29], [35] have addressed MRTA problems involving multi-robot tasks. The MRTA problem was introduced to the MARL community as a benchmark in [29], where the authors released a Python package called Level-Based Foraging (LBF) [29]. In LBF, each object is assigned a level, and it can only be picked up by a group of robots if the sum of the robots’ levels meets or exceeds the object’s level. Although LBF has become a popular MARL benchmark [36]–[38], it lacks support for dynamic object spawning and abstract action spaces (e.g., selecting task positions on the grid). In [36], several MARL algorithms were evaluated across popular benchmarks, including LBF (in fully observable scenarios only), and the EPyMARL package was released for community use. We expand their implementation by incorporating robot communication and additional features, which are detailed further in §IV.

In [34], [35], MARL is applied to an extended version of MRTA, where robots must not only collect objects but also transport them. In [35], which involves multi-robot tasks, the authors propose a novel inter-robot communication architecture. However, their approach assumes a fully observable environment. In [34], the environment is defined using a multi-channel, grid-like observation space under partial observability, with the robots’ policy modeled using a convolutional neural network, similar to our approach. However, unlike our work, they do not employ an abstract action space and use a shallower policy architecture.

III. PROBLEM DESCRIPTION

We consider a rectangular environment represented as a 2D grid with dimensions $(W \times W)$, bounded by walls on all sides, where robots and tasks are distributed, as illustrated in Fig. 2. Each cell p in the grid belongs to the cell space $\mathbb{P} = \{1, \dots, W\} \times \{1, \dots, W\}$ and can be either empty or occupied by a robot, a task, or a wall. The grid contains a homogeneous team of N robots, where the position of the i -th robot at time step t is denoted as $p_{i,t} \in \mathbb{P}$. At each t , a robot can either remain in its current position or move to an adjacent cell, including diagonal moves. Robots observe the cells within their view range, defined by R_{view} cells, and communicate with others within a communication range of R_{comm} cells.

Each task is associated with a positive integer $l_i \in \{1, \dots, L_{\text{max}}\}$, referred to as the task’s *level*, which represents the number of robots required to execute it. Here, L_{max} denotes the maximum task level. We consider a dynamic task set: tasks are removed from the environment once completed by robots, and new tasks can appear at any time step in unoccupied cells. At any time step t , the set of available tasks is represented as $\mathbb{T}_t = \{(q_i, l_i)\}_{i=1}^{T_t}$, where q_i denotes

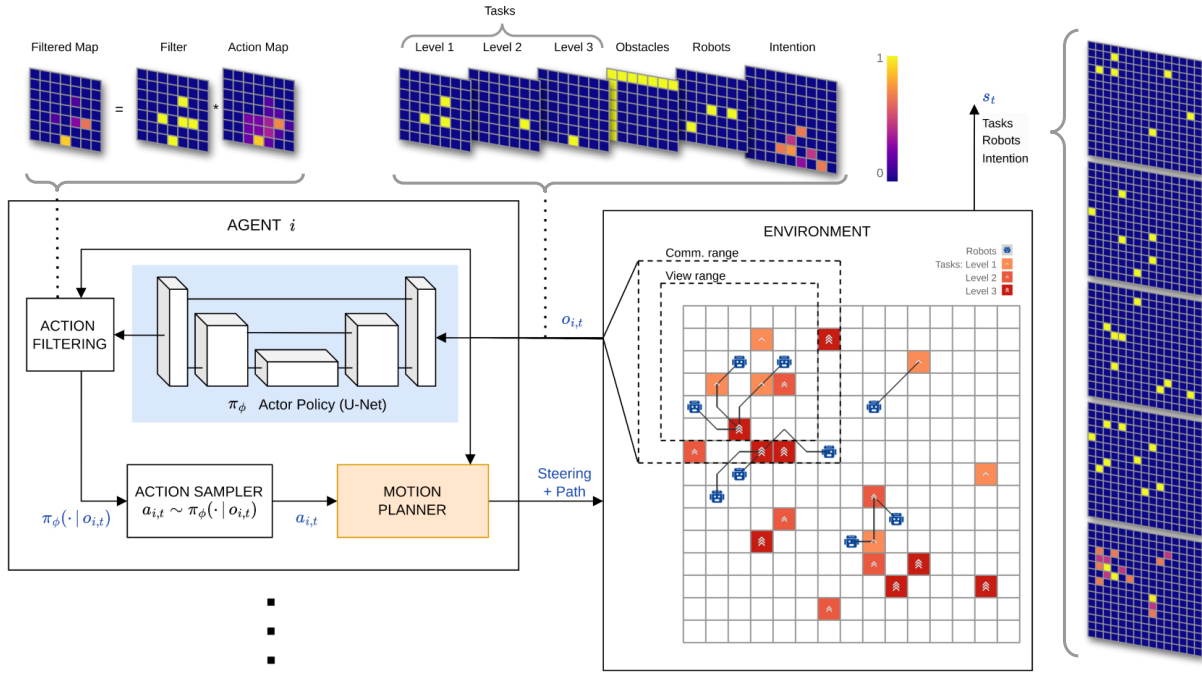


Fig. 2: Overview of the robot-environment interaction cycle. On the right a depiction of the environment is shown, along with the state representation used by the critic during training. An observation is given to each robot, where each channel encodes a different type of occupation. The observation is processed by the policy π_ϕ and filtered such that only visible tasks are considered. A task is selected from the distribution and the motion planner finds a feasible path to it. The first step along the path is fed to the environment, and the cycle repeats.

the location of the i -th task, l_i indicates its level, and T_t represents the total number of tasks available at time t .

We consider two task spawn settings: (i) *Bernoulli* (p) *spawn*: At each time step t , at each unoccupied cell, a new task can appear with probability p . The level of each newly spawned task is sampled from a discrete uniform distribution $\mathcal{U}(\{1, \dots, L_{max}\})$, ensuring equal likelihood for all task levels. (ii) *Instant respawn*: When a task is completed, a new task of the same level immediately respawns in one of the unoccupied cells. This setting maintains a constant task density throughout the episode.

To design a decentralized policy under partial observability, we model the problem as a Decentralized Partially-Observable Markov Decision Process (Dec-POMDP) [39], [40]. A Dec-POMDP is defined by the tuple $(N, \mathcal{S}, \mathcal{A}, \mathcal{T}, \mathcal{O}, O, R)$, where N is the number of robots, \mathcal{S} represents the state space of the environment, and \mathcal{A} and \mathcal{O} denote the action and observation spaces of individual robots, respectively. The state transition function $\mathcal{T} : \mathcal{S} \times \mathcal{S} \times \mathcal{A}^N \rightarrow \mathbb{R}_+$ defines the probability $\mathcal{T}(s_{t+1}|s_t, \mathbf{a}_t)$ of transitioning to the next state $s_{t+1} \in \mathcal{S}$, given the current state $s_t \in \mathcal{S}$ and the joint action $\mathbf{a}_t \in \mathcal{A}^N$ of all robots. The observation function $O : \mathcal{S} \times \{1, \dots, N\} \rightarrow \mathcal{O}$ provides each robot i with an observation $o_{i,t} = O(s_t, i)$, mapping the state space \mathcal{S} and robot index i to the observation space \mathcal{O} . Lastly, the shared reward function is represented by $R : \mathcal{S} \times \mathcal{A}^N \rightarrow \mathbb{R}$, where $r_t = R(s_t, \mathbf{a}_t)$.

Each robot i independently selects an action $a_{i,t}$ based on its policy $\pi : \mathcal{O} \times \mathcal{A} \rightarrow \mathbb{R}_+$. State-action trajectories in a Dec-POMDP are typically represented as an episode $\xi := (s_0, \mathbf{a}_0, s_1, \mathbf{a}_1, s_2, \mathbf{a}_2, \dots, s_T)$. Given an initial state

distribution $P_0 : \mathcal{S} \rightarrow \mathbb{R}_+$ and the episode likelihood $P_\pi(\xi) = P_0(s_0) \prod_{t=0}^{T-1} \prod_{i=0}^{N-1} \pi(a_{i,t}|o_{i,t}) \mathcal{T}(s_{t+1}|s_t, \mathbf{a}_t)$, the performance of a policy π can be evaluated using the expected episodic reward $\mathbb{E}_{\xi \sim P_\pi(\cdot)} [\sum_{t=0}^T \gamma^t R(s_t, \mathbf{a}_t)]$, where γ is the discount factor and T is the terminal time.

IV. TASK ALLOCATION POLICY FOR DYNAMIC COALITION FORMATION

The main contributions of this work are twofold: the development of decentralized task allocation policy models and the design of a learning-based algorithm within the Dec-POMDP framework to identify the optimal policy for the proposed models. Both aspects are elaborated in detail in this section. Our proposed policy model is designed to select tasks for execution, assess whether a robot's current task allocation requires revision, and determine new task assignments based on the robot's evolving local information. Once a task is assigned, each robot executes low-level control inputs to move along a collision-free path to a neighboring cell of its assigned task within a single time step. In the subsequent time step, the policy reassesses the task allocation based on updated local information, redirecting the robot to a new task if necessary. This iterative process ensures that the overall collective objective is optimized.

A. Multi-Agent Proximal Policy Optimization (MAPPO)

To compute the optimal policy, we adopt MAPPO [27], a CTDE algorithm designed for MARL. MAPPO enables robots to share experiences during the learning phase, which is particularly beneficial for training policies in teams of homogeneous robots. MAPPO is an Actor-Critic algorithm

comprising two distinct networks: the actor π_ϕ and the critic V_θ . The actor outputs a distribution over actions based on each robot’s observations, formally defined by the policy $\pi_\phi : \mathcal{O} \times \mathcal{A} \rightarrow \mathbb{R}_+$, where ϕ represents the parameters of the policy network. These parameters ϕ are shared across all robots, a technique known as *parameter sharing* [41], which improves training efficiency, especially in cooperative scenarios involving homogeneous robots. The critic computes an approximate value function $V_\theta : \mathcal{S} \rightarrow \mathbb{R}$, parameterized by θ , to estimate the expected discounted sum of future rewards. This is expressed as $\mathbb{E}[\sum_{\tau=t}^T \gamma^{\tau-t} R(s_\tau, \mathbf{a}_\tau)]$.

The critic V_θ is trained to accurately estimate future rewards, while the actor π_ϕ is trained to select actions that maximize the critic’s estimate. In our framework, both the actor π_ϕ and the critic V_θ are implemented using U-Nets [9], a Convolutional Neural Network (CNN)-based architecture. For this implementation, the actor’s input (observations) and output (action distribution) as well as the critic’s input (state), are represented as images (3D arrays). The U-Net architecture is particularly advantageous due to its ability to capture both local spatial relationships and global context within the input image, making it well-suited for policy learning.

B. Dec-POMDP and Task Allocation Policy Model

1) *Reward Function*: Higher-level tasks, which require coalitions of multiple robots, are more challenging to complete. To prevent robots from favoring lower-level tasks, we incentivize higher-level tasks by rewarding robots with a value equal to the square of the task level. Specifically, the reward is defined as $r_t = \sum_{i \in \mathbb{C}_t} l_i^2$, where $\mathbb{C}_t = \mathbb{T}_t \setminus \mathbb{T}_{t+1}$ represents the set of tasks completed at time step t , and l_i denotes the level of task i .

2) *State and Observation Spaces*: We adopt a 2D occupancy grid representation segmented into multiple channels (see Table I), enabling the use of CNN architectures for policy design, similar to approaches in [17], [23], [34]. This differs from the representation used in LBF [29], which encodes the state as a vector of robots and their positions. In our method, the state is defined as multiple separate channels as $s_t \triangleq (C_t^{\text{robot}}, C_t^{\text{task}}, C_t^{\text{obs}}, C_t^{\text{intent}})$, where $C_t^{\text{intent}} = C_{1,t}^{\text{intent}} \times \dots \times C_{N,t}^{\text{intent}}$ ¹.

The observation $O(s_t, i)$ for robot i is derived by projecting and cropping s_t onto areas centered around the robot’s position, determined by its view range R_{view} and communication range R_{comm} . Specifically, the robot intention channel C_t^{intent} includes $C_{j,t}^{\text{intent}}$ from robot j if j is within R_{comm} of robot i . Meanwhile, the other channels, $C_t^{\text{robot}}, C_t^{\text{task}}, C_t^{\text{obs}}$, are cropped based on R_{view} .

3) *Action Space, Motion Planner, and Intention Map*: Following a similar representation as in [17], [18], a robot’s action – determined by the task allocation policy π_ϕ – is defined as the location of its next task. Robots can select task locations only if they are within its view range; otherwise all

¹To simplify the design and enhance parameter efficiency in training the critic model, the input channel C_t^{intent} is implemented as a single aggregated channel that combines the intention channels of all robots.

TABLE I: Description of CNN channels.

Notation	Space	Description
C_t^{robot}	$\{0, 1\}^{W \times W}$	Robots
C_t^{task}	$\{0, 1\}^{W \times W \times L_{\text{max}}}$	Tasks (separated by level)
C_t^{obs}	$\{0, 1\}^{W \times W}$	Obstacles
$C_{i,t}^{\text{intent}}$	$\mathbb{R}_+^{W \times W}$	Robot i ’s intention map

Algorithm 1: Robot Motion Control

```

1 Function MotionPlanning( $p_{i,t}, a_{i,t}$ ):
2   Using the A* algorithm, find a collision-free path
   ( $\bar{p}_1, \dots, \bar{p}_n$ ) where  $\bar{p}_1 = p_{i,t}$  and  $\bar{p}_n = a_{i,t}$ .
3   return ( $\bar{p}_1, \dots, \bar{p}_n$ )
4 Procedure NextRobotPosition( $p_{i,t}, o_{i,t}$ ):
5    $a_{i,t} \sim \pi_\phi(\cdot | o_{i,t})$  // draw a task location
   using the learned policy  $\pi_\phi$  with local
   observation  $o_{i,t}$ .
6   ( $\bar{p}_1, \dots, \bar{p}_n$ ) = MotionPlanning( $p_{i,t}, a_{i,t}$ )
7    $p_{i,t+1} \leftarrow \bar{p}_2$  // assign  $\bar{p}_2$  as the robot’s
   next position to move to.
8   return  $p_{i,t+1}$ 

```

grid locations are available for task location selection. This constraint provides prior information, potentially reducing training time while encouraging robots to commit to specific tasks. By sharing task allocation information with neighboring robots, this approach facilitates coalition formation and improves overall performance.

After selecting a task location, a motion planner computes the shortest collision-free path to that location while avoiding other robots, obstacles, and other tasks. Although various approaches could be deployed, we adopt the A* search algorithm for simplicity. The path is dynamically recomputed whenever a potential collision is detected. Robots follow these updated paths to their assigned task locations. To improve coalition formation for higher-level tasks, the policy π_ϕ assigns actions by considering the long-term task execution plans of neighboring robots. Algorithm 1 outlines the motion control process for each robot guided by the learned policy π_ϕ .

We also employ an *intention map* [23] that encodes each robot’s task location and collision-free path. This intention map is shared among neighboring robots to facilitate coalition formation. Inspired by the encoding scheme in [23], we use an exponentially decaying path representation, where the i -th position on the path is weighted by $e^{-\alpha i}$, with $\alpha \geq 0$, and embedded in the intention map.

C. Learning Task Allocation and Revision

As illustrated in Fig. 2, we design a task allocation policy that assigns a task location $a_{i,t}$ to each robot based on its local information: $a_{i,t} \sim \pi_\phi(\cdot | o_{i,t})$, where $o_{i,t} = O(s_t, i)$. In a partially observable environment with dynamically spawning tasks, a robot may encounter new tasks and other robots as it moves, which were previously unaccounted for. This dynamic nature makes it challenging for multiple robots to form coalitions for higher-level tasks. Consequently, the

policy must allow robots to revise their task execution plans when necessary. However, frequent task revisions can disrupt coalition formation and hinder the completion of higher-level tasks.

To address this challenge, we enhance the MAPPO framework to train a policy capable of performing both task allocation and revision. The policy is trained to evaluate whether a robot’s current task allocation requires adjustment based on evolving local observations and information shared by neighboring robots. As demonstrated in §V, this integrated approach enables our framework to concurrently learn task allocation and revision, ensuring optimization of the overall objective in the Dec-POMDP environment.

Unlike existing approaches [22], [23], where task revisions occur only after a robot reaches its assigned task location and either completes it or fails due to the lack of a coalition, our trained policy proactively reallocates tasks whenever appropriate. In §V, we evaluate the performance improvements achieved by incorporating this task revision scheme compared to scenarios where such a scheme is absent.

V. EVALUATION

We conducted a series of simulations to evaluate (i) the performance of our proposed framework compared to existing methods, including the state-of-the-art market-based approach Project Manager-oriented Coalition Formation Algorithm (PCFA),² (ii) its scalability with respect to the number of robots, and (iii) its generalizability across a range of diverse environments. Furthermore, we present an ablation study to underscore the critical role of task revision in dynamic coalition formation.

A. Simulation Setup and Performance Metric

To evaluate our proposed method, we developed *Gym-MRTA*³, a Gym environment for discrete-space, discrete-time MRTA, and extended the existing MAPPO implementation from the EPyMARL [36] package. Our extensions include features such as task revision, action filtering, multi-dimensional observation and action spaces, support for custom state space, and tailored actor and critic Neural Network (NN) architectures. The hyperparameters of MAPPO, presented in Table IIIa, remain constant across all simulations. Each episode is limited to 100 time steps ($T = 99$) to ensure a finite episodic reward.

At the start of each episode, the initial positions of robots and tasks are randomly sampled. The environment is categorized based on task distribution as either homogeneous or non-homogeneous. In the homogeneous scenario, tasks are evenly distributed, maintaining a constant density across the grid. Conversely, the non-homogeneous scenario features uneven task distribution, resulting in variations in task density. Table II details the initial number of tasks per level across multiple task settings used in simulations.

²The original PCFA [8] was modified to account for robots with limited view and communication ranges and to enable task reassignment. Details on these modifications are provided in the Appendix.

³Our code will be made available soon.

In our simulations, we examined both homogeneous and non-homogeneous task distributions. Among the various possible non-homogeneous configurations, we selected the *random corner patch distribution*: the grid is divided into four equal-size corner patches, and at the start of each episode, one patch is randomly chosen to contain all tasks. Within the chosen patch, task density remains constant, while it is zero elsewhere. This setup evaluates whether the policy enables robots to cooperate in task execution while effectively locating tasks.

The primary performance metric is the average episodic reward. We calculate the mean and standard deviation of the episodic reward across 480 episodes: 5 different seeds with 96 evaluation episodes per seed. Each seed initializes the policy and environment with different parameters (θ, ϕ , and initial locations of robots and tasks) to ensure results are not biased by any specific initialization.

B. Results

We conducted a series of simulations to evaluate the proposed framework and the baseline across various environment settings, characterized by different task spawn configurations and task distributions, while keeping other parameters constant. A summary of all parameters is provided in Table IIIb. In the homogeneous task distribution scenario, the task spawning area is four times larger than in the non-homogeneous case. To maintain consistent robot and task densities across both distributions, the number of robots and tasks is proportionally increased by a factor of four in the homogeneous case. For this analysis, we specifically focused on the M2 and 4xM2 settings, as detailed in Table II.

Fig. 3 compares the performance of our model, the baseline (PCFA), and various ablation studies on the components of our model for both non-homogeneous and homogeneous task distributions. Table IIIc presents an overview of the models examined in this simulation, highlighting their components and referencing relevant existing works associated with these models. Each model was trained in a setting-specific manner, spanning five task spawn configurations (Bernoulli spawn with probabilities $p = 0.01, 0.02, 0.03, 0.04$ and instant respawn) for each task distribution.

Models I, II, and III in this study are relevant to existing works in the literature ([34], [17], and [23], respectively), but with notable distinctions: (i) all three models are trained using MAPPO (CTDE) within a Dec-POMDP framework, unlike other works that rely on the MDP assumption with individual rewards; (ii) while [17] focuses on individual-robot training scenarios, Model II is trained for MRTA; (iii) in [23],

TABLE II: Task settings.

Setting Name	Tasks		
	1	2	3
Easy			
E1	15	-	-
E2	10	-	-
E3	5	5	-
Medium			
M1	6	4	4
M2	4	3	3
M3	2	2	1
Hard			
H1	-	5	5
H2	-	-	10
H3	-	-	5
Homogeneous			
4xM2	16	12	12

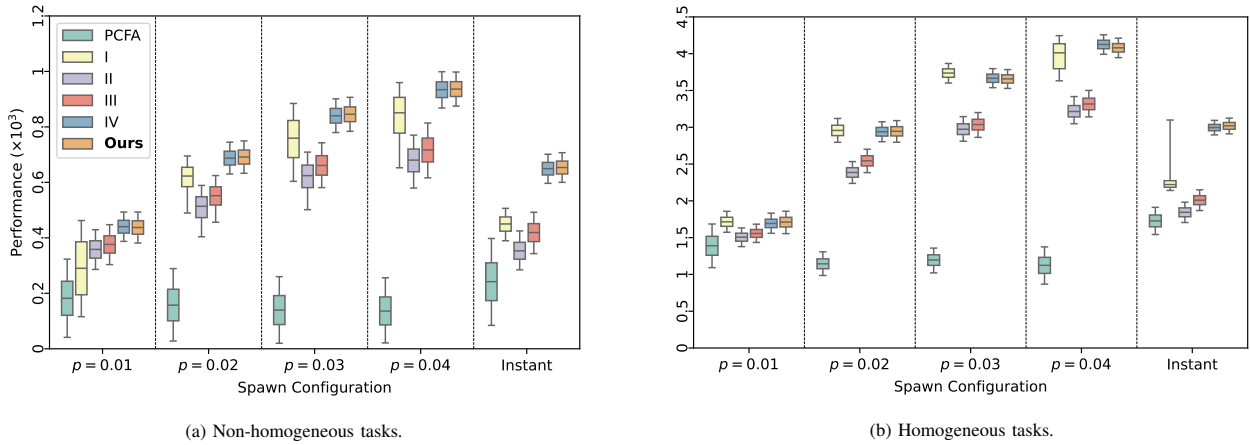


Fig. 3: Setting-specific performance across various spawn configurations.

TABLE III

(a) MAPPO Parameters.			(b) Default environment settings.			(c) Model definitions and corresponding work.					
Parameter	Value	Description	Parameter	Value(s)		Name	Components				Related Work
							Action Filtering	Spatial Actions	Intention Sharing	Task Revision	
η	$5 \cdot 10^{-4}$	Learning rate	Grid size	20 x 20		PCFA	✓		✓	✓	[8]
γ	0.95	Discount factor	View range	5		I	✓				[34]
T_{ret}	5	Adv. estimation steps	Comm. range	8		II	✓	✓			[17]
ϵ -clip	0.2	Clipping in PPO loss	Task spawn	Instant respawn / Bernoulli ($p = \{0.01, \dots, 0.04\}$)		III	✓	✓	✓		[23]
c_s	0.01	Entropy coefficient	Task distribution	Random corner patch Homogeneous		IV	✓	✓		✓	-
Batch size	10		Number of agents	10	40	Ours	✓	✓	✓	✓	-
Buffer size	10		Initial task setting (see Table II)	M2	4xM2						
Reward norm.	Yes										
Return norm.	No										

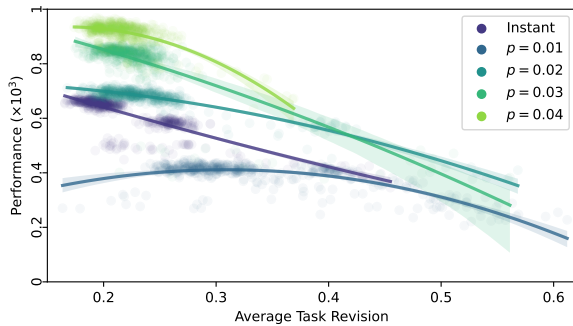


Fig. 4: The performance of the proposed framework is analyzed in relation to the average task revision rate, with data points collected over the last 500,000 training steps for each task spawn scenario. As shown, the robots gradually learn an optimal task revision strategy during training, resulting in enhanced overall performance.

only level-1 tasks are considered, and an algorithm similar to Independent Q-Learning (IQL) [42], which encourages competition rather than cooperation, is used instead of MAPPO.

Our method consistently outperforms PCFA in all configurations. Notably, as the spawn rate p increases, PCFA’s performance declines, suggesting that it struggles to coordinate robots to prioritize and allocate tasks effectively across varying levels of complexity, despite its use of multiple communication rounds to reach consensus at each step.

We observe that task revision significantly enhances performance, particularly in highly dynamic settings such as instant respawn and Bernoulli spawn with $p = 0.04$. These findings align with our expectation that, in environments

where tasks spawn frequently and dynamically, robots must plan for long-term task execution while continuously re-assessing and updating their plans. While frequent adjustments to task execution plans might intuitively seem disruptive to coalition formation among multiple robots working on high-level tasks, our proposed method enables robots to learn an optimal task revision strategy, ultimately leading to superior performance. Fig. 4 further demonstrates how our model effectively learns this strategy across various task spawn settings.

We also conducted ablation studies to evaluate the impact of intention sharing and task revision on our model’s performance. Models without task revision are limited to selecting a new task only upon reaching assigned tasks, regardless of whether it executes the tasks or not. As shown in Fig. 3, Model II (without intention sharing or task revision) underperforms both Model III (with intention sharing only) and Model IV (with task revision only), highlighting the importance of learning the optimal timing for task revision and its communication with neighboring robots. The performance difference between Models III and IV suggests that, in task allocation scenarios requiring coalition formation, determining the optimal timing for task revision is essential.

In the case of a homogeneous task distribution, Model I performs comparably to our model across all Bernoulli spawn settings but underperforms in the instant respawn scenario. This outcome suggests that homogeneous task scenarios with Bernoulli spawn do not necessitate long-term planning. However, in the instant respawn scenario,

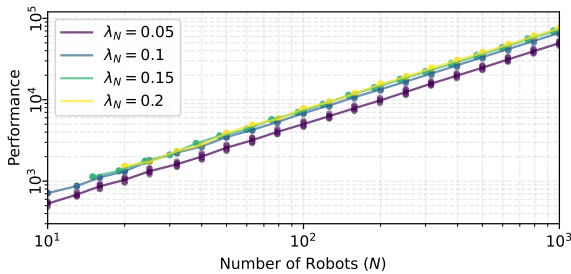


Fig. 5: Our model’s performance vs. number of robots.

the constant task density discourages simplistic approaches like those employed by Model I, resulting in its reduced performance.

C. Scalability and Generalizability Evaluation

To evaluate scalability, we first trained policies in a homogeneous task distribution environment with a fixed number of robots. The trained policy was then evaluated in environments with progressively larger numbers of robots, while proportionally scaling the environment size W and the number of tasks to maintain constant robot density ($\lambda_N = N/W^2$) and task density ($\lambda_{T,t} = T_t/W^2$), where T_t represents the number of tasks available at time t . The training environment settings were consistent with the homogeneous task simulation but utilized a smaller grid size ($W = 10$). Only the instant respawn scenario (where T_t remains constant over t) was explored, using the M2 task setting (see Table II), and multiple robot densities were considered: $\lambda_N \in \{0.05, 0.1, 0.15, 0.2\}$.

Fig. 5 illustrates the performance of trained policies as a function of $N \in [10, 1000]$. We observe that the policy’s performance scales linearly with N for all robot densities evaluated. These findings validate the scalability of our method, demonstrating its effectiveness in managing larger numbers of robots for task allocation within proportionally scaled environments.

To evaluate the generalizability of our method across environments with varying task settings, we train and evaluate our model on a diverse set of environments, each characterized by different task distributions and levels. As detailed in Table II, we designed nine task settings, categorized as easy, medium, or hard, each defined by a specific combination of task levels and quantities.

To evaluate the performance of trained policies across different task settings, we introduce the *generalizability score*. This score is calculated as the average of normalized rewards achieved by each trained policy within a specific category. The normalized reward is defined as the policy’s average reward in a given setting, scaled by the maximum

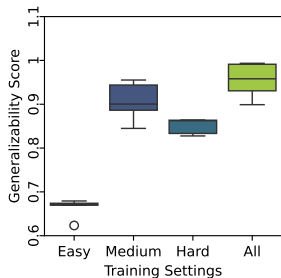


Fig. 6: Generalizability results.

attainable reward. The maximum reward is estimated based on the average reward achieved by a policy trained specifically for that setting. Consequently, a policy with strong generalizability will achieve the score closer to 1.

Fig. 6 presents the generalizability scores of policies trained in easy, medium, and hard task settings, as well as in a setting combining all three. We observe that the policy trained across all settings can generalize better and more consistently. This indicates that this policy performs close to the highest performance that setting-specific policies can attain. Based on these results, we conclude that our method enables trained policies to allow robots to achieve near-optimal performance across environments with different task level distributions when trained in diverse environment settings.

VI. CONCLUSIONS

In this work, we introduced a learning-based framework to address decentralized dynamic coalition formation. By leveraging the MAPPO algorithm and incorporating spatial action maps, motion control, task allocation revision, and intention sharing, our model demonstrated significant performance improvements over existing approaches. Extensive simulation studies highlighted the scalability of our framework with an increasing number of robots and its generalizability, performing well across diverse environments.

Future directions include enhancing the learning algorithm by integrating learned communication strategies (instead of predefined intention-based communication) and incorporating mechanisms for achieving consensus among robots, particularly for bandwidth-abundant environments.

APPENDIX

Modifications to PCFA: We implemented PCFA and integrated it with *GymRTA* for the performance comparison. To ensure a fair comparison with our method, the following modifications are applied:

- **Partial Observability:** In PCFA, the utility function for a task is set to zero if the task lies outside the robot’s view range R_{view} , preventing robots from forming coalitions for tasks they cannot observe. Additionally, the communication graph is updated at each time step, with links existing only between robots that are within the communication range R_{comm} .
- **Task Assignment Revision:** To align with our method, robots are allowed to revise their task assignments at every time step. This is achieved by recomputing all four stages of PCFA at every time step. While this modification increases communication overhead compared to the original PCFA, it enables a fair comparison.

The utility function was adjusted to align with the reward function used in our framework:

$$s_k(t_{\text{ETA}}) = l_k^2 e^{-2(t_{\text{ETA}} + t_w - t_k^0)},$$

where l_k is the task level, t_{ETA} is the estimated time of arrival, t_w is the wait time, and t_k^0 is the task’s initial spawn time.

The modified PCFA implementation is available in our code repository.

REFERENCES

- [1] B. P. Gerkey and M. J. Mataric, "A formal analysis and taxonomy of task allocation in multi-robot systems," *The International Journal of Robotics Research*, vol. 23, no. 9, pp. 939–954, 2004.
- [2] E. Tuci, M. H. Alkilabi, and O. Akanyeti, "Cooperative object transport in multi-robot systems: A review of the state-of-the-art," *Frontiers Robotics AI*, vol. 5, p. 335700, 5 2018.
- [3] C. Mouradian, J. Sahoo, R. H. Glitho, M. J. Morrow, and P. A. Polakos, "A coalition formation algorithm for multi-robot task allocation in large-scale natural disasters," *2017 13th International Wireless Communications and Mobile Computing Conference, IWCMC 2017*, pp. 1909–1914, 7 2017.
- [4] M. S. Couceiro, D. Portugal, J. F. Ferreira, and R. P. Rocha, "Semfire: Towards a new generation of forestry maintenance multi-robot systems," *Proceedings of the 2019 IEEE/SICE International Symposium on System Integration, SII 2019*, pp. 270–276, 4 2019.
- [5] A. Khamis, A. Hussein, and A. Elmogy, "Multi-robot task allocation: A review of the state-of-the-art," *Studies in Computational Intelligence*, vol. 604, pp. 31–51, 2015.
- [6] F. Quinton, C. Grand, and C. Lesire, "Market approaches to the multi-robot task allocation problem: a survey," *Journal of Intelligent & Robotic Systems*, vol. 107, 2 2023.
- [7] H. L. Choi, L. Brunet, and J. P. How, "Consensus-based decentralized auctions for robust task allocation," *IEEE Transactions on Robotics*, vol. 25, pp. 912–926, 2009.
- [8] G. Oh, Y. Kim, J. Ahn, and H. L. Choi, "Market-based task assignment for cooperative timing missions in dynamic environments," *Journal of Intelligent and Robotic Systems: Theory and Applications*, vol. 87, pp. 97–123, 7 2017.
- [9] W. Weng and X. Zhu, "U-net: Convolutional networks for biomedical image segmentation," *IEEE Access*, vol. 9, pp. 16591–16603, 5 2015.
- [10] S. Park, Y. D. Zhong, and N. E. Leonard, "Multi-robot task allocation games in dynamically changing environments," *Proceedings - IEEE International Conference on Robotics and Automation*, vol. 2021-May, pp. 13415–13422, 2021.
- [11] S. Park and J. Barreiro-Gomez, "Payoff mechanism design for coordination in multi-agent task allocation games," *2023 62nd IEEE Conference on Decision and Control (CDC)*, pp. 8116–8121, 2023.
- [12] S. Park, "Tuning rate of strategy revision in population games," *2023 American Control Conference (ACC)*, pp. 423–428, 5 2023.
- [13] G. Notomista, S. Mayya, S. Hutchinson, and M. Egerstedt, "An optimal task allocation strategy for heterogeneous multi-robot systems," *2019 18th European Control Conference, ECC 2019*, pp. 2071–2076, 6 2019.
- [14] A. Prorok, M. A. Hsieh, and V. Kumar, "The impact of diversity on optimal control policies for heterogeneous robot swarms," *IEEE Transactions on Robotics*, vol. 33, no. 2, pp. 346–358, 2017.
- [15] S. Singh, A. Srikanthan, V. Mallampati, and H. Ravichandar, "Concurrent Constrained Optimization of Unknown Rewards for Multi-Robot Task Allocation," in *Proceedings of Robotics: Science and Systems*, 2023.
- [16] B. Xie, S. Chen, J. Chen, and L. C. Shen, "A mutual-selecting market-based mechanism for dynamic coalition formation," *International Journal of Advanced Robotic Systems*, vol. 15, 2 2018.
- [17] J. Wu, X. Sun, A. Zeng, S. Song, J. Lee, S. Rusinkiewicz, and T. Funkhouser, "Spatial action maps for mobile manipulation," *Robotics: Science and Systems*, 4 2020.
- [18] F. Xia, C. Li, R. Martín-Martín, O. Litany, A. Toshev, and S. Savarese, "Relmogen: Leveraging motion generation in reinforcement learning for mobile manipulation," *Proceedings - IEEE International Conference on Robotics and Automation*, vol. 2021-May, pp. 4583–4590, 8 2020.
- [19] A. Nagabandi, K. Konolige, S. Levine, and V. Kumar, "Deep dynamics models for learning dexterous manipulation," in *Conference on Robot Learning*, pp. 1101–1112, PMLR, 2020.
- [20] C. Sun, J. Orvik, C. M. Devin, B. H. Yang, A. Gupta, G. Berseth, and S. Levine, "Fully autonomous real-world reinforcement learning with applications to mobile manipulation," in *Conference on Robot Learning*, pp. 308–319, PMLR, 2022.
- [21] A. Agrawal, A. S. Bedi, and D. Manocha, "Rtaw: An attention inspired reinforcement learning method for multi-robot task allocation in warehouse environments," *Proceedings - IEEE International Conference on Robotics and Automation*, vol. 2023-May, pp. 1393–1399, 9 2022.
- [22] A. Krnjaic, R. D. Stealec, J. D. Thomas, G. Papoudakis, L. Schäfer, A. W. K. To, K.-H. Lao, M. Cubuktepe, M. Haley, P. Børsting, and S. V. Albrecht, "Scalable multi-agent reinforcement learning for warehouse logistics with robotic and human co-workers," in *IEEE/RSJ International Conference on Intelligent Robots and Systems*, 2023.
- [23] J. Wu, X. Sun, A. Zeng, S. Song, S. Rusinkiewicz, and T. Funkhouser, "Spatial intention maps for multi-agent mobile manipulation," *Proceedings - IEEE International Conference on Robotics and Automation*, vol. 2021-May, pp. 8749–8756, 3 2021.
- [24] S. V. Albrecht, F. Christianos, and L. Schäfer, *Multi-Agent Reinforcement Learning: Foundations and Modern Approaches*. MIT Press, 2024.
- [25] S. Omidshafiei, J. Papis, C. Amato, J. P. How, and J. Vian, "Deep decentralized multi-task multi-agent reinforcement learning under partial observability," *34th International Conference on Machine Learning, ICML 2017*, vol. 6, pp. 4108–4122, 3 2017.
- [26] J. Foerster, N. Nardell, G. Farquhar, T. Afouras, P. H. Torr, P. Kohli, and S. Whiteson, "Stabilising experience replay for deep multi-agent reinforcement learning," *34th International Conference on Machine Learning, ICML 2017*, vol. 3, pp. 1879–1888, 2 2017.
- [27] C. Yu, A. Velu, E. Vinitzky, J. Gao, Y. Wang, A. Bayen, and Y. Wu, "The surprising effectiveness of PPO in cooperative multi-agent games," in *Proceedings of the 36th International Conference on Neural Information Processing Systems*, pp. 24611–24624, 2022.
- [28] J. N. Foerster, G. Farquhar, T. Afouras, N. Nardelli, and S. Whiteson, "Counterfactual multi-agent policy gradients," *32nd AAAI Conference on Artificial Intelligence, AAAI 2018*, pp. 2974–2982, 5 2017.
- [29] F. Christianos, L. Schäfer, and S. V. Albrecht, "Shared experience actor-critic for multi-agent reinforcement learning," *Advances in Neural Information Processing Systems*, vol. 2020-December, 6 2020.
- [30] T. Rashid, M. Samvelyan, C. Schroeder, G. Farquhar, J. Foerster, and S. Whiteson, "QMIX: Monotonic value function factorisation for deep multi-agent reinforcement learning," in *International Conference on Machine Learning*, pp. 4295–4304, PMLR, 2018.
- [31] P. Sunehag, G. Lever, A. Gruslyns, W. M. Czarnecki, V. Zambaldi, M. Jaderberg, M. Lanctot, N. Sonnerat, J. Z. Leibo, K. Tuyls, *et al.*, "Value-decomposition networks for cooperative multi-agent learning based on team reward," in *Proceedings of the 17th International Conference on Autonomous Agents and MultiAgent Systems*, pp. 2085–2087, 2018.
- [32] H. Zhou, T. Lan, and V. Aggarwal, "PAC: Assisted value factorization with counterfactual predictions in multi-agent reinforcement learning," *Advances in Neural Information Processing Systems*, 2022.
- [33] R. Lowe, Y. Wu, A. Tamar, J. Harb, P. Abbeel, and I. Mor-datch, "Multi-agent actor-critic for mixed cooperative-competitive environments," *Advances in Neural Information Processing Systems*, vol. 2017-December, pp. 6380–6391, 6 2017.
- [34] S. Shaw, E. Wenzel, A. Walker, and G. Sartoretti, "Formic: Foraging via multiagent rl with implicit communication," *IEEE Robotics and Automation Letters*, vol. 7, pp. 4877–4884, 6 2020.
- [35] K. Shibata, T. Jimbo, T. Odashima, K. Takeshita, and T. Matsubara, "Learning locally, communicating globally: Reinforcement learning of multi-robot task allocation for cooperative transport," *IFAC-PapersOnLine*, vol. 56, no. 2, pp. 11436–11443, 2023.
- [36] G. Papoudakis, F. Christianos, L. Schäfer, and S. V. Albrecht, "Benchmarking multi-agent deep reinforcement learning algorithms in cooperative tasks," in *Proceedings of the Neural Information Processing Systems Track on Datasets and Benchmarks (NeurIPS)*, 2021.
- [37] J. Cao, L. Yuan, J. Wang, S. Zhang, C. Zhang, Y. Yu, and D. C. Zhan, "Linda: multi-agent local information decomposition for awareness of teammates," *Science China Information Sciences*, vol. 66, pp. 1–17, 8 2023.
- [38] K. Boggess, S. Kraus, and L. Feng, "Toward policy explanations for multi-agent reinforcement learning," *IJCAI International Joint Conference on Artificial Intelligence*, pp. 109–115, 4 2022.
- [39] F. A. Oliehoek and C. Amato, *A Concise Introduction to Decentralized POMDPs*. Springer, 2016.
- [40] D. V. Pynadath and M. Tambe, "The communicative multiagent team decision problem: Analyzing teamwork theories and models," *Journal Of Artificial Intelligence Research*, vol. 16, pp. 389–423, 6 2001.
- [41] J. K. Gupta, M. Egorov, and M. Kochenderfer, "Cooperative multi-agent control using deep reinforcement learning," in *Autonomous Agents and Multiagent Systems*, vol. 10642 LNAI, pp. 66–83, Springer, 2017.
- [42] M. Tan, "Multi-agent reinforcement learning: independent versus cooperative agents," in *Proceedings of the Tenth International Conference on International Conference on Machine Learning*, p. 330–337, 1993.